JACC: BASIC TO TRANSLATIONAL SCIENCE VOL. 5, NO. 12, 2020
© 2020 THE AUTHORS. PUBLISHED BY ELSEVIER ON BEHALF OF THE AMERICAN COLLEGE OF CARDIOLOGY FOUNDATION. THIS IS AN OPEN ACCESS ARTICLE UNDER THE CC BY-NC-ND LICENSE (http://creativecommons.org/licenses/by-nc-nd/4.0/).

PRECLINICAL RESEARCH

In Situ Remodeling Overrules Bioinspired Scaffold Architecture of Supramolecular Elastomeric Tissue-Engineered Heart Valves

Marcelle Uiterwijk, MD,[a,*] Anthal I.P.M. Smits, PhD,[b,c,*] Daphne van Geemen, PhD,[b] Bas van Klarenbosch, MD,[d] Sylvia Dekker, MSc,[b] Maarten Jan Cramer, MD, PhD,[d] Jan Willem van Rijswijk, MSc,[a] Emily B. Lurier, PhD,[b,e] Andrea Di Luca, PhD,[b] Marieke C.P. Brugmans, PhD,[f] Tristan Mes, PhD,[g] Anton W. Bosman, PhD,[g] Elena Aikawa, MD, PhD,[h] Paul F. Gründeman, MD, PhD,[i] Carlijn V.C. Bouten, PhD,[b,c,†] Jolanda Kluin, MD, PhD[a,c,†]

VISUAL ABSTRACT

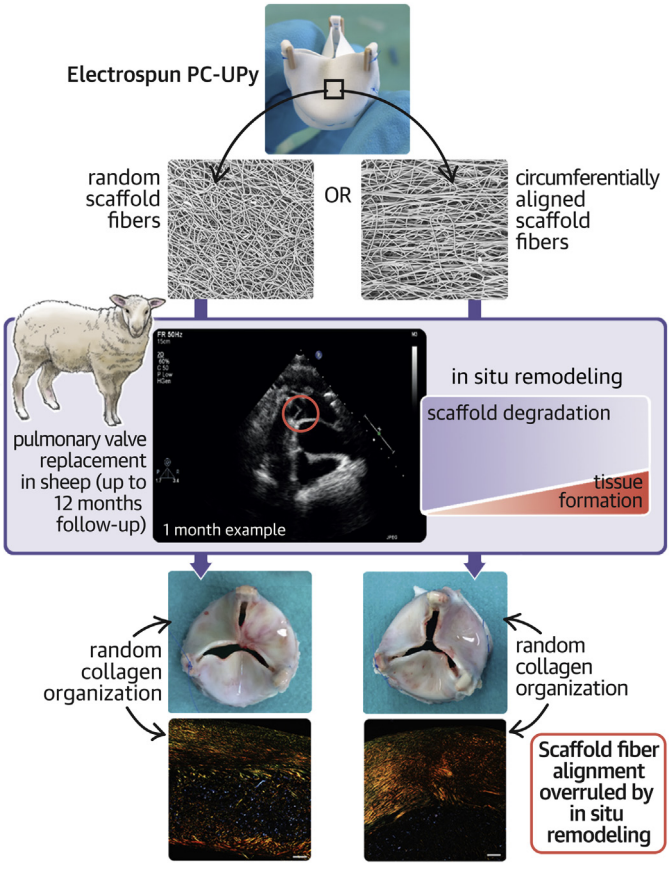

Uiterwijk, M. et al. J Am Coll Cardiol Basic Trans Science. 2020;5(12):1187–206.

HIGHLIGHTS

- **The predefined fiber alignment in electrospun biodegradable heart valve scaffolds did not lead to consistent collagen organization in the predefined direction.**
- **A tendency for higher regurgitation rate and peak gradient was seen in the aTEHVs.**
- **Biaxial tensile tests on the explanted aTEHVs revealed loss of mechanical integrity of the circumferentially aligned fibers after 1 month.**
- **Isotropic mechanical properties were seen in all explanted scaffolds at 6 and 12 months.**
- **Valve-to-valve variability was observed, regardless of the study group, both on the macroscopic and microscopic levels.**

ISSN 2452-302X https://doi.org/10.1016/j.jacbts.2020.09.011

JACC: BASIC TO TRANSLATIONAL SCIENCE VOL. 5, NO. 12, 2020
DECEMBER 2020:1187–206

ABBREVIATIONS AND ACRONYMS

aTEHV = anisotropic tissue-engineered heart valve

GPC = gel permeation chromatography

rTEHV = random tissue-engineered heart valve

SEM = scanning electron microscopy

TEHV = tissue-engineered heart valve

TTE = transthoracic echocardiography

SUMMARY

In situ tissue engineering that uses resorbable synthetic heart valve scaffolds is an affordable and practical approach for heart valve replacement; therefore, it is attractive for clinical use. This study showed no consistent collagen organization in the predefined direction of electrospun scaffolds made from a resorbable supramolecular elastomer with random or circumferentially aligned fibers, after 12 months of implantation in sheep. These unexpected findings and the observed intervalvular variability highlight the need for a mechanistic understanding of the long-term in situ remodeling processes in large animal models to improve predictability of outcome toward robust and safe clinical application. (J Am Coll Cardiol Basic Trans Science 2020;5:1187–206)
© 2020 The Authors. Published by Elsevier on behalf of the American College of Cardiology Foundation. This is an open access article under the CC BY-NC-ND license (http://creativecommons.org/licenses/by-nc-nd/4.0/).

Heart valves are living, dynamic tissues. In both pulmonary and aortic valvular leaflets, the organization of the collagen network in the fibrosa layer remodels from a more random direction in embryonic and early postnatal stages into a highly anisotropic, circumferentially aligned fibrous network during childhood and adulthood (1). This structural anisotropy results in a mechanical anisotropy that is essential for proper valve functionality (2,3). Disruptions of the collagen organization are associated with valve pathologies and dysfunction (4).

Replacement of diseased valves with the current clinically available nonviable valve prostheses leads to a compromised quality of life and reduced life expectancy. The use of cell-free bioresorbable heart valve prostheses has been proposed to overcome the intrinsic limitations of traditional valve prostheses (5–7). These types of prosthetic valves are designed to trigger endogenous regeneration of the valve, directly in situ (7,8). The approach of in situ tissue-engineered heart valves (TEHVs) relies on endogenous colonization of the implanted valve prosthesis by host cells, followed by tissue formation and remodeling, whereas the implanted valvular scaffold is gradually resorbed (8,9). Although there are some data on the in situ tissue engineering of heart valves using natural materials, such as decellularized allografts, xenografts (10–12), or decellularized de novo engineered matrixes (13–18), the availability of long-term in vivo data on resorbable synthetic heart valves is currently limited [for a detailed overview on TEHVs, please see Mela et al. (19)].

Recently, a preclinical study demonstrated the proof of concept for this technology using electrospun valvular scaffolds based on resorbable supramolecular elastomers (5). In this study, the organization of the newly formed collagen displayed a predominant orientation in the radial direction, if any, rather than the native-like circumferential collagen orientation. Mimicking the native extracellular matrix organization via endogenous regeneration in situ remains a challenge due to the lack of understanding of the remodeling processes that drive in situ valvular regeneration. In an in vitro study, Foolen et al. (20) reported on the competition between contact guidance and strain avoidance, which suggested a dominant influence of contact guidance on cellular orientation in a collagenous matrix. De Jonge et al. (21) demonstrated that contact guidance exerted by electrospun scaffold fibers resulted in cellular alignment and collagen deposition parallel to the electrospun fibers. However, it is unknown how fiber organization of a resorbable valvular scaffold influences collagen alignment and tissue regeneration processes in vivo.

The goal of this study was to investigate the influence of a predefined scaffold fiber alignment in the

From the [a]Department of Cardiothoracic Surgery, Amsterdam University Medical Center, Amsterdam, the Netherlands; [b]Department of Biomedical Engineering, Eindhoven University of Technology, Eindhoven, the Netherlands; [c]Institute for Complex Molecular Systems, Eindhoven University of Technology, Eindhoven, the Netherlands; [d]Department of Cardiology, University Medical Center Utrecht, Utrecht, the Netherlands; [e]School of Biomedical Engineering, Science and Health Systems, Drexel University, Philadelphia, Pennsylvania, USA; [f]Xeltis B.V., Eindhoven, the Netherlands; [g]SupraPolix B.V., Eindhoven, the Netherlands; [h]Center for Excellence in Vascular Biology, Division of Cardiovascular Medicine, Brigham and Women's Hospital, Harvard Medical School, Boston, Massachusetts, USA; and the [i]Department of Cardiothoracic Surgery, University Medical Center Utrecht, Utrecht, the Netherlands. *Drs. Uiterwijk and Smits contributed equally to this work. †Drs. Bouten and Kluin contributed equally to this work.
The authors attest they are in compliance with human studies committees and animal welfare regulations of the authors' institutions and Food and Drug Administration guidelines, including patient consent where appropriate. For more information, visit the Author Center.

Manuscript received March 18, 2020; revised manuscript received September 22, 2020, accepted September 22, 2020.

circumferential direction in electrospun resorbable synthetic pulmonary heart valves on valve functionality and the in situ formation and organization of new tissue. We hypothesized that a bio-inspired scaffold fiber orientation (i.e., circumferentially aligned) would induce native-like matrix formation, with collagen deposition in the direction of the scaffold fibers due to contact guidance, which would improve valve function and durability.

METHODS

VALVE PREPARATION AND SURGICAL IMPLANTATION. We manufactured electrospun tri-leaflet valve scaffolds of ureidopyrimidinone-polycarbonate with either a random fiber alignment (rTEHV) or with fibers with a predominant alignment in the circumferential direction of the valve leaflet (aTEHV). Electrospun tubular conduits were sutured onto a crown-shaped polyether ether ketone supporting ring (outer diameter 20 mm, inner diameter 18 mm) to create a tri-leaflet valvular shape (**Figures 1A and 1B**), as previously described in detail (5). The scaffold microstructure was analyzed via scanning electron microscopy (SEM), and fiber alignment was quantified according to previously described algorithms (22). In vitro valve functionality was evaluated in a hydrodynamic pulsatile duplicator system under physiological pulmonary conditions in accordance with the International Organization of Standardization norms. The valves were sterilized by gamma irradiation (25 kGy; Synergy health, Venlo, the Netherlands). Subsequently, 20 adult female Swifter sheep underwent surgical orthotopic pulmonary valve replacement. The animal experiments were approved by the Animal Care Ethics committee of the University Medical Centre Utrecht and were performed in agreement with the current Dutch law on animal experiments. Animals received Ascal (1 daily dose [dd] 80 mg orally; Ratiopharm, Ulm, Germany) for 3 months. The scheduled follow-up period was 1 month (n = 2), 6 months (n = 4), and 12 months (n = 4) in each group.

VALVE EVALUATIONS. We evaluated native cardiac functionality using echocardiography at time of implantation (transthoracic echocardiography [TTE]). At time of implantation and explantation, the functionality of TEHVs was evaluated with epicardial echocardiography (under full anesthesia). During follow-up, TTE was performed (at 2, 4, 6, and 9 months) in the animal dome while the animals were fully awake. The explanted valves were macroscopically evaluated, carefully resected from the polyether ether ketone reinforcement ring, and transected for further analysis according to a predefined cutting scheme (Supplemental Figure S1). Collagen organization was evaluated by picrosirius red staining on longitudinal valve sections, imaged with polarized light. En face collagen alignment was assessed by confocal laser scanning microscopy. The mechanical properties of the explanted valves and the nonimplanted control scaffolds were determined via biaxial tensile tests. Scaffold fiber resorption was qualitatively analyzed with SEM and quantified in terms of molecular weight by gel permeation chromatography (GPC) on samples treated with sodium hypochlorite (Clorox) to remove the tissue and expose the remaining scaffold fibers. Tissue formation and cellularization were assessed comprehensively by histology, SEM, biochemical assays (DNA, collagen, elastin, and glycosaminoglycans). Mineral deposition was analyzed with Von Kossa staining. Details of the methods are reported in the Supplemental Appendix.

STATISTICS. Values are reported as the mean ± SD per group or as median (25th and 75th percentiles). Statistical analyses was performed (in cases, $n > 6$) after testing for normality using the d'Agostoni and Pearson omnibus test (GraphPad, La Jolla, California). Pre-implantation scaffold characteristics were compared between rTEHVs and aTEHVs via unpaired Student's *t*-test (aligned fiber fractions) or nonparametric unpaired Student's *t*-tests (Mann-Whitney) (scaffold thickness and fiber diameter). Baseline characteristics for the animal experiments at the time of implantation (animal weight, native pulmonary valve annulus) were compared between groups (rTEHV vs. aTEHV) using an unpaired Student's *t*-test. Due to the low sample size, changes in animal weight were only evaluated by comparing measurements of all animals with the baseline weight using the Wilcoxon test (nonparametric paired Student's *t*-test). Changes in leaflet length were evaluated between time points using a nonparametric unpaired Student's *t*-test (Mann-Whitney). The chi-square test was used for comparing leaflet mobility (good vs. reduced) as qualitatively analyzed by echocardiography (SPSS version 25, IBM, Armonk, New York). Statistical analysis for the biochemical assays and GPC measurements were not taken into consideration because of the limited sample numbers. Differences were considered statistically significant at $p < 0.05$.

FIGURE 1 Scaffold Characterization Before Implantation

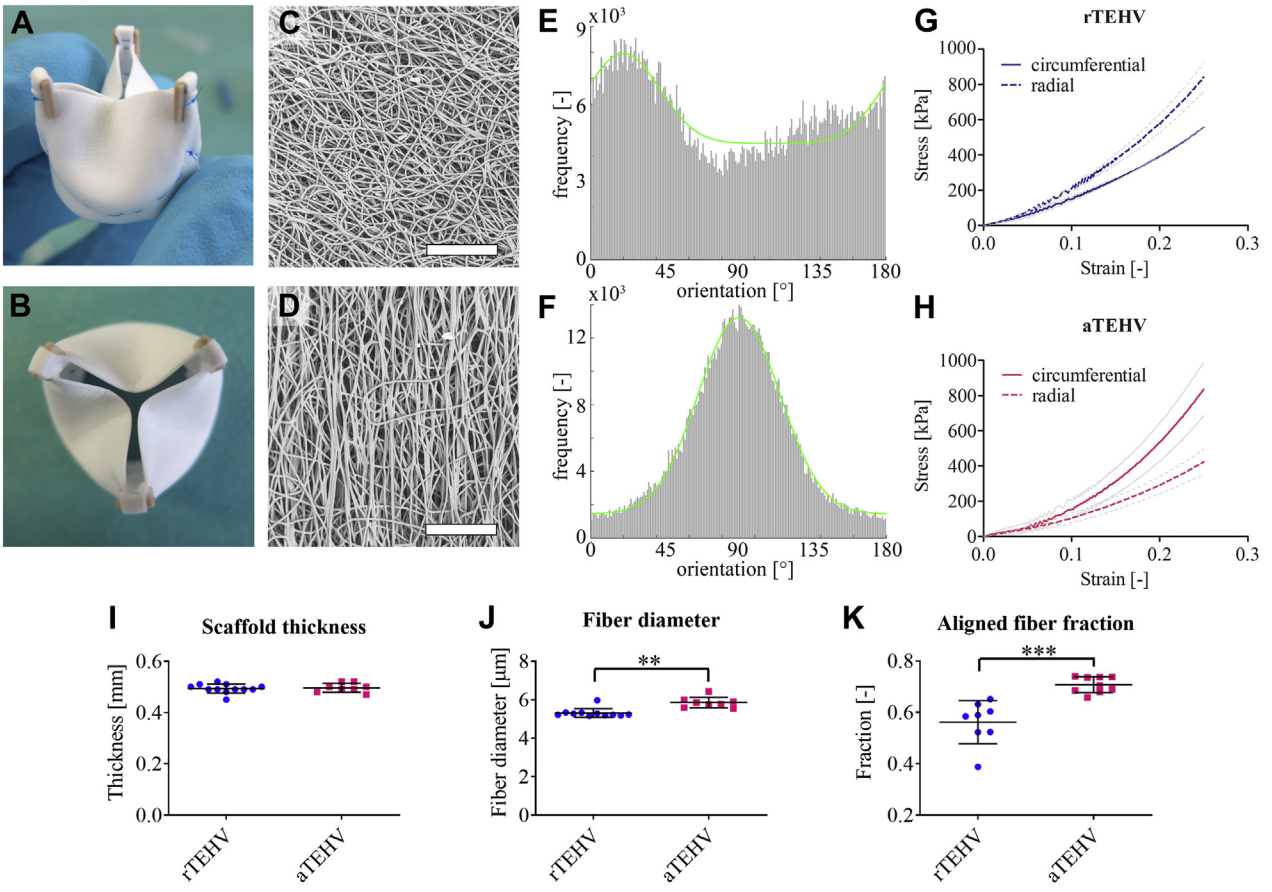

(A and B) Photographs of an electrospun valve after suturing onto the supporting ring. **(C and D)** Scanning electron microscopy (SEM) images of the electrospun scaffolds with **(C)** random or **(D)** circumferentially aligned fibers. Scale bars, 200 μm. **(E and F)** Orientation histograms of the **(E)** random and **(F)** aligned scaffolds showing the frequencies of fibers at angles between 0 and 180 degrees, with an angle of 0 degrees representing the radial direction and 90 degrees representing the circumferential direction of the valve leaflet. A Gaussian curve with an additional baseline was fitted through the data **(green curves)**, which was used to determine the principal fiber angle and the aligned fiber fraction. **(G and H)** Average stress-strain curves (± SD in **gray**) in the circumferential **(solid lines)** and radial direction **(dashed lines)** for the **(G)** random (random tissue-engineered heart valve [rTEHVs]) and **(H)** aligned valves (anisotropic tissue-engineered heart valve [aTEHVs]). **(I)** Average scaffold thickness, **(J)** fiber diameter, **(K)** and aligned fiber fraction for rTEHVs **(blue)** and aTEHVs **(red)**. **p < 0.01; ***p < 0.001.

RESULTS

FABRICATION OF HEART VALVE SCAFFOLDS WITH CIRCUMFERENTIAL FIBER ORGANIZATION AND ANISOTROPIC MECHANICAL BEHAVIOR. SEM analysis displayed a highly porous fibrous micro-architecture for both rTEHV and aTEHV scaffolds (Figures 1C and 1D). The average scaffold thickness was 0.5 ± 0.02 mm for both scaffolds (Figure 1I). The average fiber diameter was slightly larger for the aTEHVs compared with the rTEHVs (5.9 ± 0.3 μm vs. 5.3 ± 0.2 μm; p = 0.002) (Figure1J). Quantification of the extent of fiber alignment revealed a strong predominant fiber alignment in the circumferential direction in the aTEHVs (Figure 1F). In contrast, the rTEHVs displayed a main fiber orientation in the radial direction (Figure 1E). However, the extent of fiber alignment in the rTEHVs was significantly less pronounced than that of the aTEHVs, as was evident from the significantly lower aligned fiber fraction for rTEHVs (0.56 ± 0.03 vs. 0.71 ± 0.01; p < 0.001) compared with aTEHVs (Figure 1K). These results were also reflected in the mechanical properties of the valvular scaffolds, which demonstrated the highest stiffness in the radial direction for the rTEHVs and the highest stiffness in the circumferential direction for the aTEHVs before implantation (Figures 1G and 1H). In vitro functionality tests demonstrated adequate functionality for both rTEHVs and aTEHVs (Videos 1 and 2, respectively).

TABLE 1 Animal and Valve Characteristics at Time of Implantation and Explantation

	rTEHV	N	aTEHV	N	All
Implantation					
Animal weight (kg)	52.6 ± 6.0	10	51.6 ± 2.7	10	52.0 ± 4.6
Native PV annulus (mm)	25.3 ± 1.3*	10	24.1 ± 1.1*	10	24.7 ± 1.3
Explantation					
Animal weight (kg)					
1 month	51.75 (51.50–52.00)	2	52.5 (48.0–57.0)	2	53.3 (48.7–57.8)
6 months	57.75 (53.6–62.3)	4	55.0 (54.6–56.5)	4	55.3 (54.6–59.3)†
12 months	64.3 (58.6–72.9)	4	68.0 (61.5–74.5)	2	64.3 (60.4–74.8)‡
TEHV leaflet length (mm)					
1 month	9.6 (–)	1	11.26 (10.52–11.99)	2	10.52 (9.61–11.99)
6 month	11.17 (9.45–11.74)	3	10.54 (9.81–10.96)	4	10.7 (9.82–11.40)
12 month	8.96 (7.46–10.13)	4	9.20 (8.45–9.96)	2	9.19 (7.84–10.02)§

Values are mean ± SD (normal distribution) or median (25th to 75th percentile). *Significant difference between random tissue-engineered heart valve (rTEHV) versus anisotropic tissue-engineered heart valve (aTEHV) ($p < 0.05$). †Significant difference between implantation and 6 months ($p = 0.008$) and ‡implantation and 12 months ($p = 0.031$). §Significant difference between 6 and 12 months ($p < 0.05$).

PV = pulmonary valve.

However, some pinning of the leaflets was observed in the aTEHVs specifically, which might have been caused by the higher stiffness and might have resulted in undesired stress concentrations. Functional readouts (effective orifice area, regurgitation fraction, leakage, and closing volume) were in accordance with International Organization of Standardization norms (Supplemental Table S1). Although the closing volume exceeded International Organization of Standardization norms, this was likely an effect of the porosity of the electrospun valves in the in vitro conditions and did not necessarily reflect the in vivo functionality, because the scaffold would be filled with fibrin from the blood instantaneously.

IN VIVO PERFORMANCE OF rTEHVs AND aTEHVs. Nineteen animals (95%) recovered well from the surgical valve implantation procedure. One animal died 1 day post-operatively due to complications in the operating room (#1.4). Two animals (both aTEHVs) were euthanized before their allocated time point due to right heart failure caused by endocarditis of their implanted valves (#12.7 and #12.8, after 1.5 and 9 months, respectively). For details of the baseline and explantation characteristics, see **Table 1**. All implanted TEHVs revealed none or mild regurgitation on epicardial echocardiography directly after implantation in the operating room. One aTEHV (#6.8) showed an immobile leaflet that was maintained during follow-up. No severe regurgitation was seen during follow-up (performed in the stable while the animals were fully awake). The aTEHVs showed a trend of earlier and higher incidence of moderate valve regurgitation in time on TTE (**Figure 2M**). However, the epicardial echocardiogram evaluation (under full anesthesia) at time of explantation was not in line with the TTE results, which showed a trend toward a higher level of valve regurgitation in the rTEHVs (**Figure 2N**). The functional data of each individual animal can be found in Supplemental Table S2. The systolic transvalvular peak pressure gradients increased over time in both groups (**Figure 2O**). The noninvasive (echo) examinations of the rTEHVs showed an overall increase of the peak gradient between 2, 6, and 12 months, with a mean from 15.2 ± 3.5 mm Hg to 21.2 ± 6.35 to 27.1 ± 8.1 mm Hg. For the aTEHVs, the mean of the peak gradient increased from 19.7 ± 4.9 mm Hg to 23.6 ± 6.83 to 34.1 mm Hg in the same period (**Figure 2O**). The invasive pressure examination in the operating room also showed an increase in the peak gradient in all animals, except 2 with rTEHVs (#6.1 and #6.2). In general, at 6 months, the rTEHV had a lower peak gradient, as did the aTEHV, which ranged from 7 to 10 mm Hg versus 15 to 23 mm Hg (Supplemental Table S3). Due to loss of 2 (50%) animals in the aTEHV group, 12-month results were not conclusive. However, overall results of the invasive and noninvasive data revealed a trend in higher pressure gradient in the aTEHVs.

Gross explantation evaluation. Macroscopic evaluation of the valves did not reveal an evident difference between the valve types (**Figure 2**, Supplemental Figures S3 to S5). After 1-month follow-up, all valves had smooth and pliable leaflets, and none of the valves showed signs of (non-)structural valve deterioration. At 6 months, 2 rTEHVs valves (#6.3 and #6.4) had smooth and pliable leaflets, whereas 2 other rTEHVs showed small (1 to 2 mm) irregularities (#6.1 and #6.2) (Supplemental Figure S6) and 1 sign of leaflet retraction (#6.2) due to tissue overgrowth and

JACC: BASIC TO TRANSLATIONAL SCIENCE VOL. 5, NO. 12, 2020
DECEMBER 2020:1187–206

FIGURE 2 **Gross Morphology and In Vivo Functionality of Random (rTEHV) and Aligned (aTEHV) TEHVS**

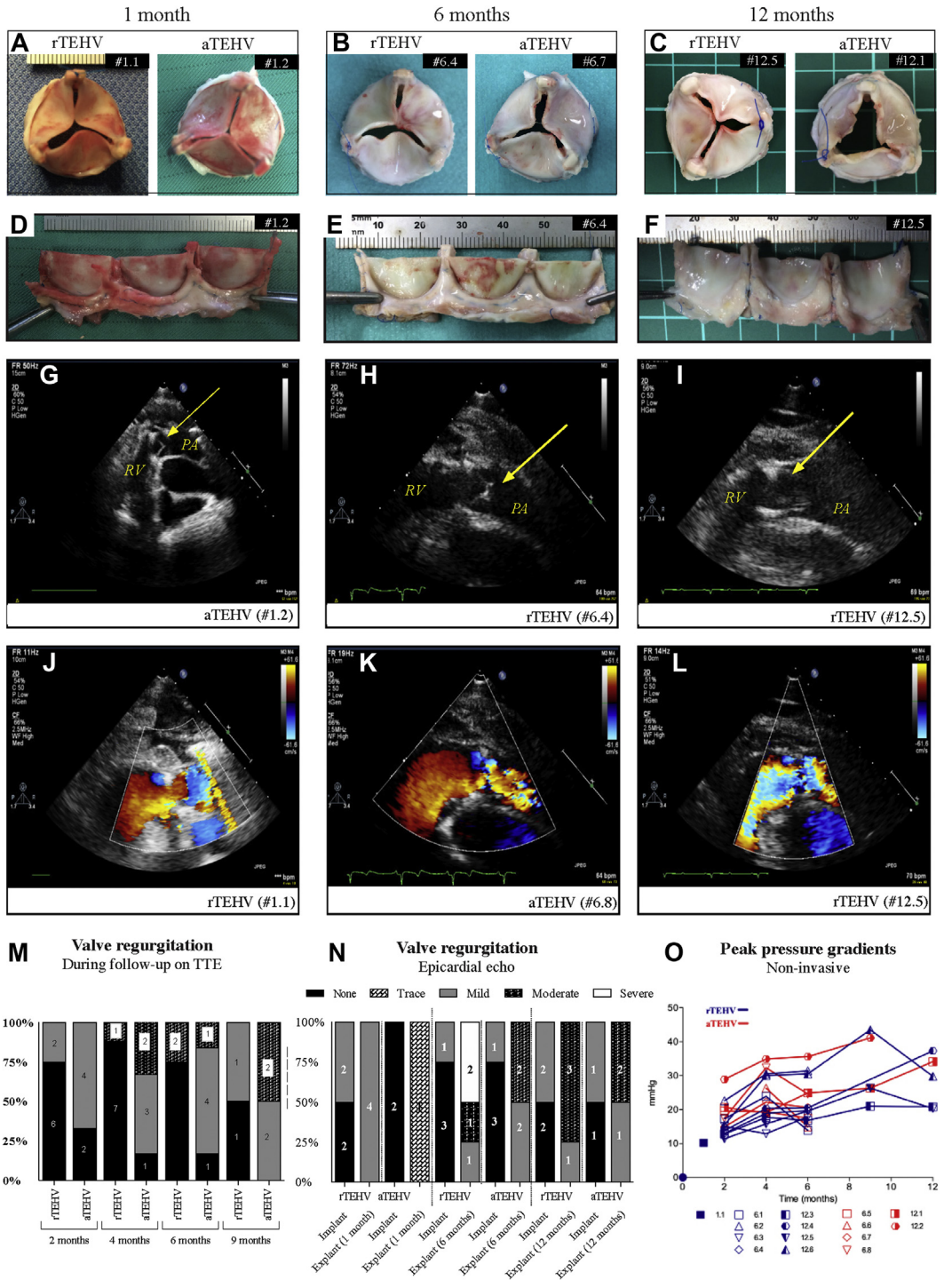

(A to C) Macroscopic images of representative valves from distal pulmonary artery view after 1, 6, and 12 months follow-up and **(D to F)** unfolded from polyether ether ketone (PEEK) stent. **(G to L)** Echocardiography demonstrating adequate opening and closing of the presented valve leaflets at 1, 6, and 12 months indicated with **yellow arrow**. **(M)** Proportion of pulmonary regurgitation of implanted TEHVs during follow-up on transthoracic echocardiography (TTE). **(N)** Epicardial echo evaluation at implantation and explantation. **(O)** Systolic peak pressure gradient during follow-up period (noninvasive measurements). PA = pulmonary artery; RV = right ventricle; other abbreviations as in Figure 1.

consequent fusion of the lateral side of the leaflet belly with the strut region. All aTEHVs showed small irregularities (range 1 to 5 mm) on their leaflets or in the commissure regions of the valves. Two aTEHVs had mild signs of leaflet retraction due to curling of the free edge to the pulmonary side (#6.6) or belly-strut fusion (#6.8). One aTEHV (#6.5) showed a 5 mm tear perpendicular to the leaflet free edge (Supplemental Figure S6). At 12 months, 3 rTEHVs (#12.3, #12.6, and #12.4) showed small irregularities on and tears in their leaflets. Moreover, a large calcified nodule ($11 \times 17 \times 11$ mm) was seen on top of a strut, connected with the pulmonary artery (#12.4) (Supplemental Figure S5). One valve in this group (#12.6) showed 2 small tears in 1 leaflet, near the struts, of 4.5 and 2.6 mm in length. Also, retraction of the leaflet due to tissue overgrowth and fusion of the belly with the strut region was seen in this valve. One rTEHV was not affected by signs of deterioration and had pliable and smooth leaflets (#12.5). Both aTEHVs at 12 months showed irregularities on their leaflets (#12.1 and #12.2). Also, mild retraction of the leaflet was seen in some due to adhesion of a small part of the ventricular side of the leaflet near the commissure with the strut region (#12.2) and/or curling of the free edge to pulmonary side (#12.1) (Supplemental Figure S6). The leaflet length (nadir: free edge) decreased from an average of 10.7 ± 1.2 mm and 10.6 ± 0.9 mm at 1 and 6 months, respectively, to an average of 9.1 ± 1.0 mm at 12 months. The decrease was significant over time ($p < 0.001$), but there was no significant difference between the groups (9.2 ± 1.1 mm vs. 8.9 ± 1.4 mm for rTEHVs and aTEHVs, respectively) (**Table 1**).

Collagen orientation. Picrosirius red staining with polarized light imaging revealed that collagen fibers with various degrees of maturity were heterogeneously distributed on top of and in the scaffold layer in both groups (**Figure 3**). No clear fiber orientation of collagen in the circumferential direction was visible in either of the groups, in contrast to the collagen fibers in native control valves, which revealed a clear circumferential alignment of collagen fibers in the fibrosa (**Figure 3B**). The collagen in the TEHVs showed a particularly chaotic organization in the hinge region. En face imaging of the superficial tissue layers on the pulmonary and the ventricular side of the leaflet using a viable fluorescent collagen probe [CNA35-mCherry (23)] revealed no apparent effect of the pre-imposed scaffold architecture on collagen organization (**Figure 4**, Supplemental Figures S7 to S9). However, although the distribution of the fibers was homogeneous in the 6-month explantations, we observed a bi-directional fiber distribution (with the radial direction as the principle direction) in the superficial tissue layers of the 12-month explantation, particularly at the pulmonary side in both groups. No consistent differences were observed between rTEHVs and aTEHVs, although there were differences in the amount and alignment of collagen deposition between the pulmonary and ventricular sides of the leaflet, as well as between valves, both within each group and between the groups. However, it should be noted that the imaging depth was limited to the superficial layers of the leaflet, which consisted of collagen deposits on top of the scaffold. Hence, contact guidance by the scaffold fibers was limited in these layers.

Biomechanical valve leaflet evaluation. At 1 month, bi-axial tensile tests revealed a remarkable decrease in the circumferential stiffness of the aTEHVs, whereas there was no change in the radial stiffness (**Figure 5A**). This resulted in a switch in the anisotropy ratios, with a value of approximately 2 for the implanted scaffolds (i.e., circumferential stiffness was twice the radial stiffness) to a value ≤ 1 at 1 month (**Figures 5G and 5H**). The mechanical properties of the 1-month rTEHV explantation were similar to those pre-operatively (**Figure 5B**). At 6 months, both types of scaffolds displayed a more nonlinear mechanical behavior, with a decreased stiffness in the low-strain regime (5% strain) (**Figures 5C and 5E**) and an increased stiffness in the high-strain regime (15% strain) (**Figures 5D and 5F**). From 6 to 12 months, the rTEHVs showed an overall decrease in stiffness (**Figures 5C and 5D**), whereas the aTEHVs showed an overall increase in stiffness (**Figures 5E and 5F**). At 6 and 12 months, the circumferential stiffness was comparable to the radial stiffness for both scaffold types, as evident from the anisotropy ratios close to a value of 1 at those time points (**Figures 5G and 5H**).

SCAFFOLD DEGRADATION AND NEOTISSUE FORMATION. Qualitative assessment of scaffold resorption over time revealed minimal fiber resorption at 1 month in both scaffold types, although minor pit formation was visible mainly in the aTEHV group (**Figures 6A and 6B**). At 6 months, extensive scaffold fiber degradation was observed in both groups. This was even more pronounced at 12 months, with extensive localized degradation of scaffold fibers. The fiber diameter did not significantly change over time in both groups, but remained slightly larger in the aTEHV group compared with the rTEHV group (**Figure 6C**). The molecular weights of the remaining scaffold material tended to decrease over time, with a slight increase in the dispersity

FIGURE 3 Collagen Alignment as Visualized by Picrosirius Red Staining With Polarized Light Microscopy

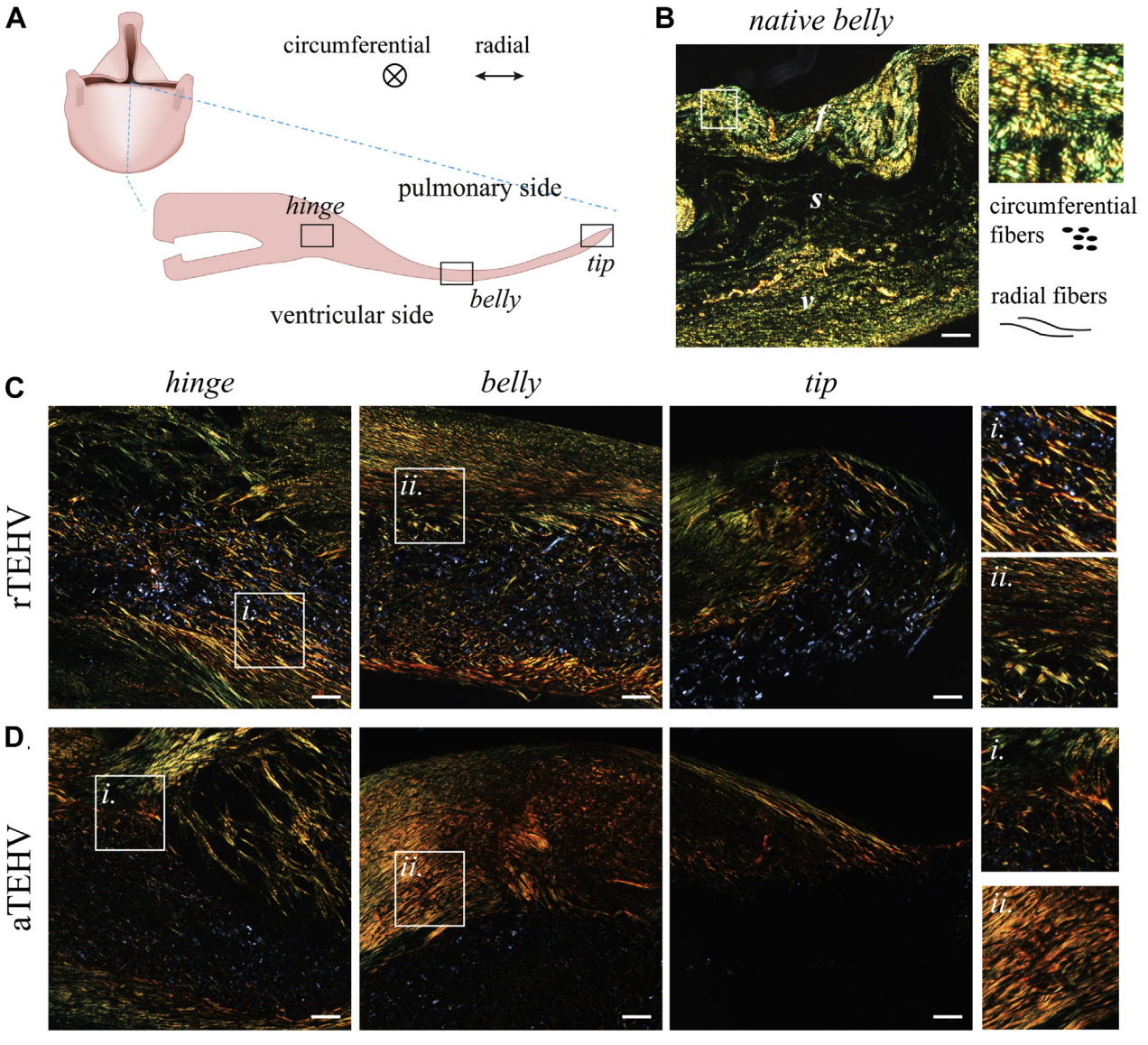

(A) Schematic representation of a longitudinal section of the valve leaflet with the respective regions indicated in the leaflet image collection, with radial and circumferential directions as indicated. (**B**) Collagen alignment in the native sheep pulmonary valve leaflet for reference, revealing the 3-layered structure with the fibrosa (f), spongiosa (s), and ventricularis (v). Circumferentially aligned fibers are oriented perpendicular to the field of view, appearing as speckle-like structures. Radially aligned fibers are oriented parallel to the field of view, appearing as fiber-like structures. (**C and D**) Representative images of collagen alignment in the hinge, belly, and tip regions of 12-month explantation in the **(C)** rTEHV and **(D)** aTEHV groups. Scale bars, 100 μm. Abbreviations as in Figure 2.

index (Figures 6D to 6F). These trends were comparable for both scaffold types, although the molecular weight of the aTEHVs was lower than that of the rTEHVs from before implantation throughout follow-up due to batch-to-batch variability in the synthesized polymer (Figures 6D and 6E).

Histopathological observations of the explanted valve leaflets revealed that synthetic scaffold fibers were present up to 12 months. At 6-month and 12-month follow-up, regions of active resorption by giant cells were observed (Figure 7G). In some cases, these active remodeling areas induced local leaflet thickening, which was predominantly observed at the hinge region of the leaflet but also visible in the belly or tip regions of the leaflet. In terms of cellularization, sparse cell populations were observed in

FIGURE 4 **En Face Imaging of Collagen Alignment in the Superficial Layers on Either Side of the Leaflet**

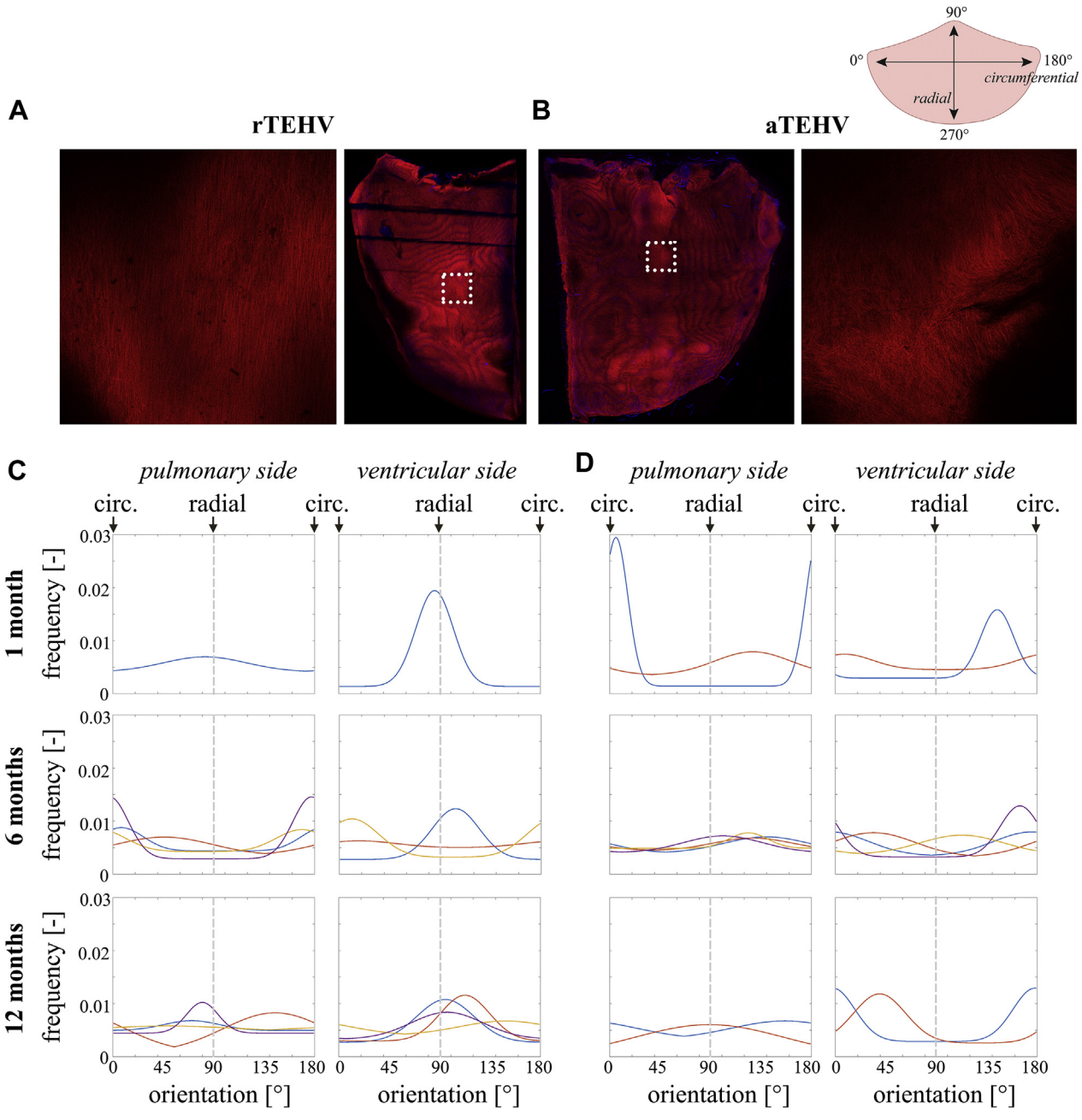

(A and B) Representative images of collagen staining (CNA35-mCherry) staining showing composed tile scans of the pulmonary side of half an **(A)** rTEHV and half an **(B)** aTEHV leaflet, with examples of individual tiles. **(C and D)** Quantification of the tile scans resulted in orientation histograms for each side of the leaflet of each individual valve. Each line represents 1 valve; 90 degrees corresponds to the radial direction; 0 degrees corresponds to the circumferential direction of the leaflet. Abbreviations as in Figure 2.

either scaffold type at 1 month, progressively increasing in density in both groups up to 6 months and becoming stabilized at 12 months (Figures 7G and 7J, Supplemental Figures S10 to S13). A higher number of cells was localized in the hinge region of the leaflets, with a relatively lower cell density in the belly and tip regions (Figure 7M). At 12 months, both aTEHVs and rTEHVs showed regions with

FIGURE 5 Explantation Mechanical Properties Over Time

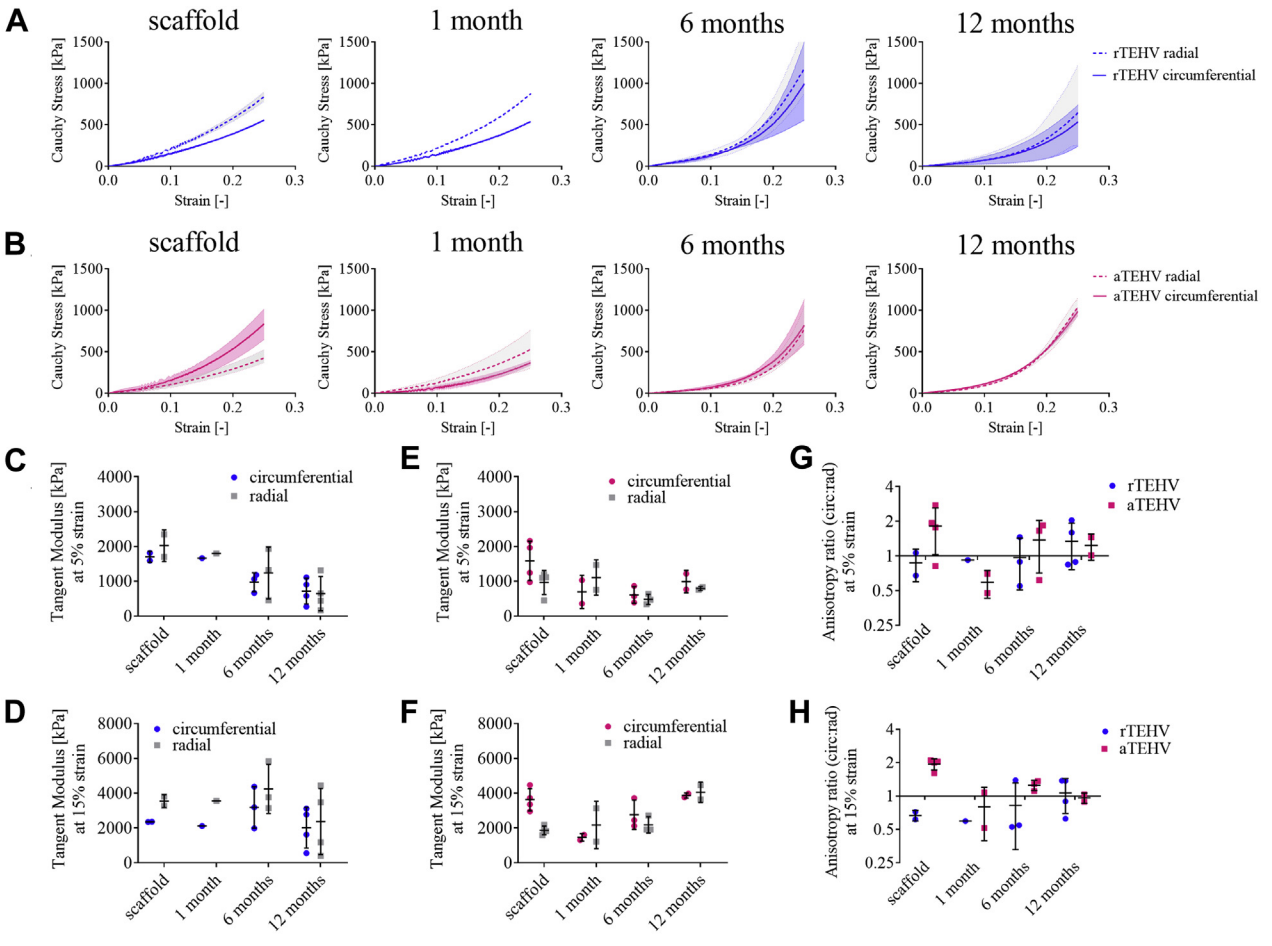

(A) Average stress-strain curves of random (rTEHV) and **(B)** aligned (aTEHV) heart valves before implantation (scaffold) and at 1, 6, and 12 months follow-up. **(C to F)** Tangent moduli in the low (5%) and high (15%) strain regions of the **(C and D)** rTEHVs and **(E and F)** aTEHVs. **(G and H)** Anisotropy ratios (circumferential stiffness/radial stiffness) at **(G)** 5% and **(H)** 15% strain. Abbreviations as in Figure 2.

multinucleated giant cells in the presence of the synthetic fibers (Supplemental Figure S14). Endothelial coverage was evident from 6 months on, and it gradually progressed to a more complete endothelium at 12 months, although exposed scaffold fibers were still visible in some valves, particularly near the free edge of the leaflet (Supplemental Figures S15 and S16). Typically, the endothelial coverage was observed to start near the hinge region. At 6 months, endothelialization was complete in all valves in this region, both on the pulmonary and the ventricular sides. In most of the valves, the endothelial coverage had also extended to the belly region at 6 months (Supplemental Figure S15), although there were valves in which small regions of scaffolds were still exposed, particularly at the ventricular side. There was more variability between valves near the tip of the leaflet, which was fully endothelialized at 6 months in a subset of the valves, whereas others still had substantial parts of the scaffold fibers exposed (e.g., valve #6.3; as also shown in Supplemental Figure S15). At 12 months, the endothelialization was more complete, with typically full coverage of the hinge and belly regions at both sides of the leaflet. Also at 12 months, the endothelialization near the leaflet tip was variable between valves and between the pulmonary and ventricular side of the leaflet. Most of the valves displayed complete endothelium at 12 months, but there were valves with patches of various sizes with exposed scaffold fibers near the tip (e.g., valves #12.4 and #12.1, as shown in

FIGURE 6 Scaffold Degradation Over Time

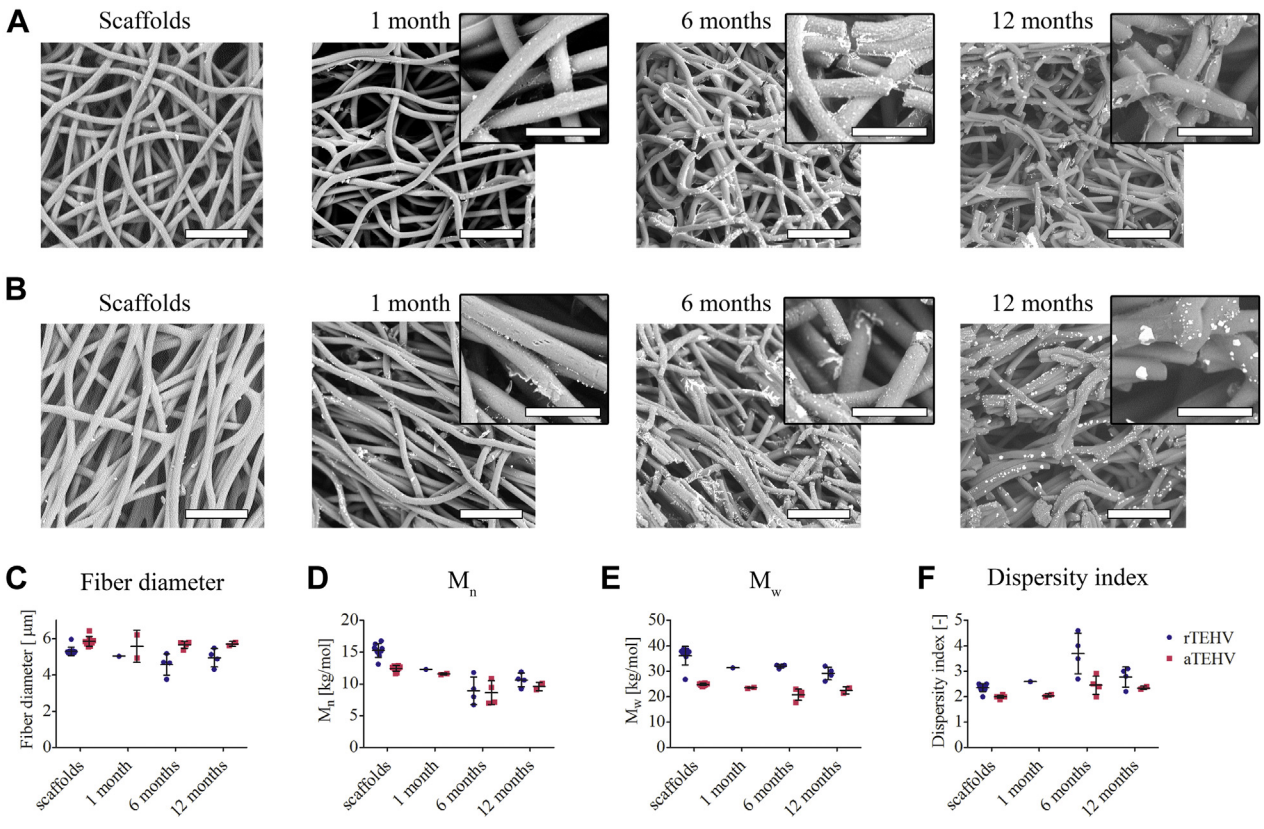

(A and B) SEM images of Clorox-treated explantations of **(A)** rTEHVs and **(B)** aTEHVs, revealing progressive resorption of scaffold fibers. Scale bars, 50 µm; scale bars insets, 20 µm. **(C)** Average fiber diameter over time, as determined from SEM images. **(D)** The number-averaged (M_n), **(E)** weight-averaged molecular weight (M_w), and **(F)** the dispersity index (M_w/M_n) over time, as determined by gel permeation chromatography. Abbreviations as in Figures 1 and 2.

Supplemental Figure S16). This was observed at either side of the leaflet.

Extracellular matrix formation, including collagen and elastin, was barely present after 1 month in both groups (**Figures 7A and 7D**, Supplemental Figures S10 and S11). At 6 months, a collagen-rich neotissue layer covered the scaffold, which was most pronounced at the pulmonary side (**Figures 7B and 7E**, Supplemental Figures S12 and S13). At 12 months, the collagen fibers started to infiltrate and replace the scaffold fibers (**Figures 7C and 7F**). Quantitative analyses did not reveal a statistically significant difference between groups or between leaflet regions for the presence of collagen (**Figure 7N**). In the neotissue layer, few and thin elastin fibers (grades 1 and 2) (Supplemental Figure S2) were detected at 6 months in both groups (Supplemental Figures S12 and S13). They appeared as small localized groups of fibrils, heterogeneously spread in the neotissue layer in all regions of the leaflets or appeared as continuous fibers at the pulmonary side. At 12 months, elastin was present, with the same appearance (stage and amount) in both groups (**Figures 7I and 7L**). Biochemical analyses of the explantation demonstrated an increase in DNA and glycosaminoglycan content in the valvular leaflets from 1 to 6 months, which remained stable up to 12 months (**Figures 8A and 8B**). Collagen (hydroxyproline) content also showed an increase from 1 to 6 months and tended to increase from 6 to 12 months in both TEHVs (**Figure 8C**). (Tropo)elastin was detected at 1 month and tended to remain constant from 6 to 12 months (**Figure 8D**).

Mineral deposition. No mineral deposition was seen in any of the explantations after 1 month of implantation. At 6 months, the rTEHV and aTEHVs explanted valves showed minor size mineral deposits (50% vs. 100%). Two (50%) aTEHVs showed macro-

FIGURE 7 **Histological Analyses of Random (rTEHVs) and Aligned (aTEHVs) Valves**

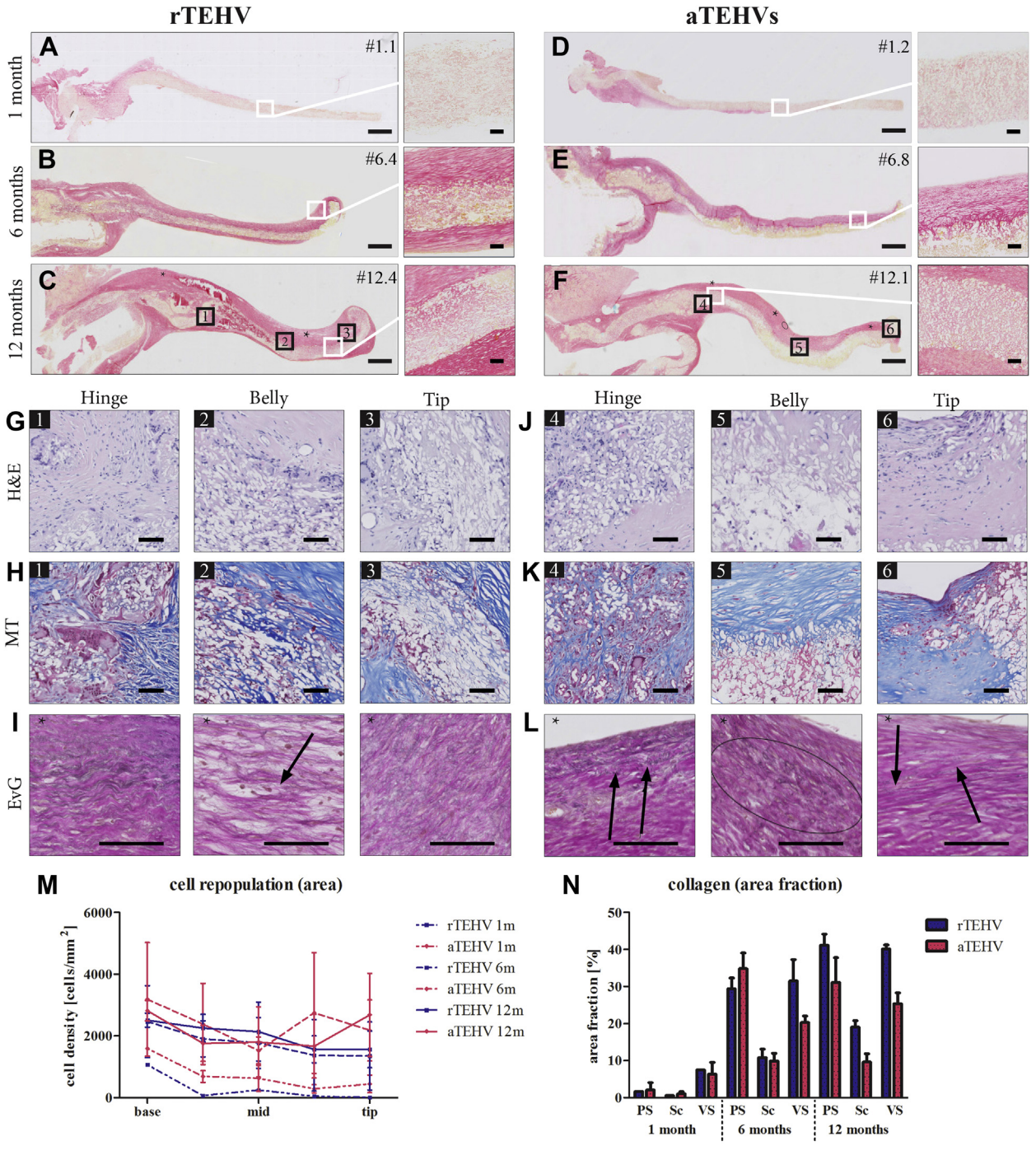

Tile scans of collagen staining (picrosirius red) of the **(A to C)** rTEHVs and **(D to F)** aTEHVs at 1, 6, and 12 months, with 20× magnification of regions of interest as indicated (scale bar tile scans, 1 mm; scale bars insets, 50 μm). **(G to L)** High-magnification images at the hinge **(1)**, belly **(2)**, and tip **(3)** regions of the 12-months explantations, showing cell infiltration in all regions of the leaflet (hematoxylin and eosin [H and E]; nuclei in **dark purple) (G and J)** and deposition of extracellular matrix components, such as collagen (Masson's trichrome [MT]; collagen in **blue**, scaffold in **white**, cytoplasm in **pink**) **(H and K)**, and elastin fibers (Elastica van Gieson [EvG]; elastin; **black arrows**) **(I and L)**. Scale bars, 50 μm. **(M)** Quantification of the cell density per leaflet region (hinge, belly, tip) over time. **(N)** Quantification of the collagen distribution over time as pannus overgrowth on the pulmonary side (PS), inside the scaffold (Sc), or on the ventricular side (VS). Abbreviations as in Figure 2.

FIGURE 8 Biochemical Composition of rTEHVS and aTEHVS

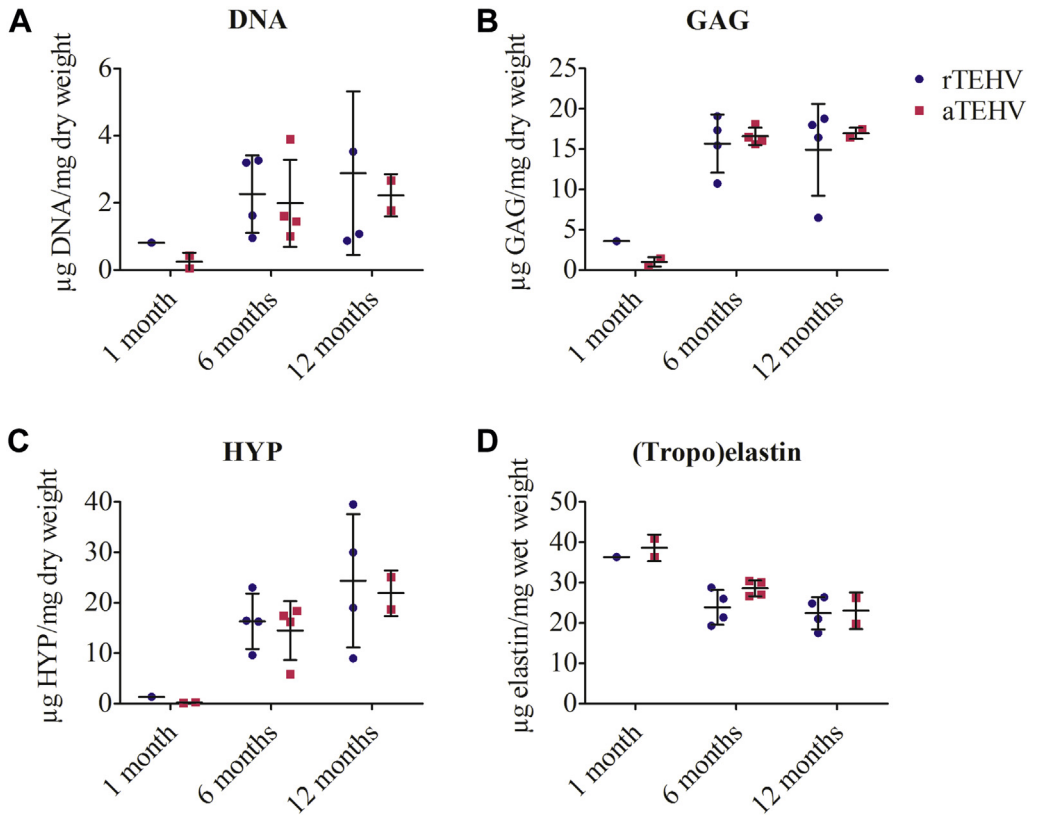

Amount of **(A)** DNA, **(B)** glycosaminoglycans (GAG), **(C)** hydroxyproline (HYP) as measures for collagen, and **(D)** (tropo) elastin. Abbreviations as in Figure 2.

sized deposits in the hinge region at this time point. At 12 months, both scaffold variants showed micro deposits. Three rTEHVs (75%) and 1 rTEHV (50%) had macro deposits in their leaflets. Micro size deposits appeared in 2 distinct morphological manifestations, namely, in a vesicle form associated with apoptotic cells or cells in osteogenic transformation process, and as small elongated deposits, which were suggested to be matrix calcifications. For details of morphological manifestation and location of the analyzed leaflet in the individual valves, see Figure 9.

DISCUSSION

In the present study, we hypothesized that, based on the principle of contact guidance, bio-inspired scaffold fiber alignment (in the circumferential direction) would induce a more native-like organization of the regenerated tissue. Surprisingly, any prefabricated mechanical anisotropy was lost in all valves after in vivo implantation. Moreover, our results did not show consistent differences in the organization of the regenerated collagen between rTEHVs and aTEHVs after long-term follow-up, and there was substantial valve-to-valve variability.

Biomechanical behavior is essential for native heart valve function, and various manufacturing techniques have been used to mimic this in prosthetic heart valves (24). The use of a nature-inspired, well-defined scaffold microstructure to guide in situ tissue regeneration was reported by various studies (18,25-29). Several studies demonstrated the ability to manufacture heart valve scaffolds with anisotropic, native-like mechanical characteristics (30-32). For example, Saidy et al. (33) recently described the development of heart valve scaffolds with a highly defined biomimicking micro-architecture using melt electrowriting. D'Amore et al. (34) reported on the fabrication of synthetic heart valve scaffolds with bioinspired geometry, microstructure, and

FIGURE 9 Mineral Deposits by Von Kossa Staining

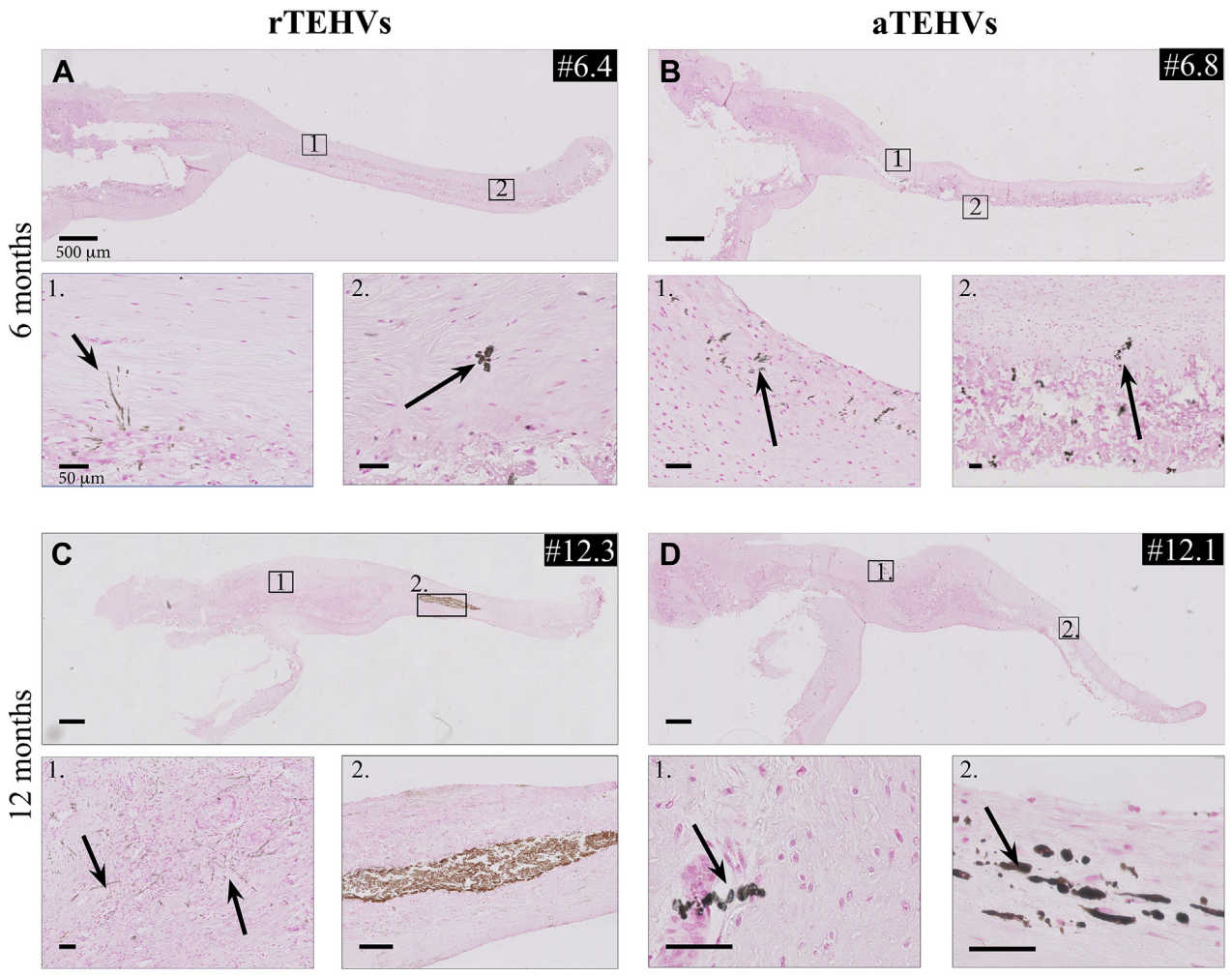

(A to D) Images of mineral deposition, indicated by **arrows**, in **(A and C)** rTEHV and **(B and D)** aTEHVs after 6- and 12-month follow-up. **Inset** shows representative examples of micro deposits, as variant A; micro noduli **(insets A2, B2, D1, and D2)** or variant B; affected extracellular matrix components **(insets A1, B1, C1)** and macro size mineral deposits **(C2)**. Individual data of mineral deposition after **(E)** 1, **(F)** 6, or **(G)** 12 months implantation, presented as color-code expression (**green**: not present and **red**: present) on the presence of micro (variant A and B) or macro size minerals deposits for different valve locations (hinge, belly, and tip). (Scale bar tile scans, 500 μm; scale bars insets, 50 μm). Abbreviations as in Figure 2.

mechanical properties using an electrodeposition technique. Short-term in vivo evaluation of bio-inspired valves was reported by Capulli et al. (29). They showed the ability to manufacture biomimetic heart valve scaffolds with anisotropic mechanical characteristics by jet-spinning of poly-4-hydroxybutyrate with gelatin. Subsequently, they evaluated the valves using a transcutaneous implantation technique and assessed functionality in an orthotopic pulmonary position in a sheep model for 15 h. Reimer et al. (18) reported on cell-free valves created from fibrin hydrogel implanted in orthotopic pulmonary position in lambs. These valves showed native-like anisotropic mechanical properties, with the modulus being approximately 4 times stiffer in the circumferential direction compared with the radial direction. The valves functioned well up to 8 weeks in vivo, after which their insufficiency index worsened due to weakness of the suture lines in the design, according to the investigators. Using computational modeling, Loerakker et al. (35) demonstrated that anisotropic mechanical properties in TEHVs, in addition to geometry, could have a profound effect on valve functionality and mechano-transduction. Moreover, Serrani et al. (36) recently described a predominant circumferential fiber alignment in

synthetic heart valve scaffolds that was optimal for valve functioning, based on an in silico model. However, none of these studies evaluated the effect of native-like scaffold architecture in heart valves on neotissue regeneration and organization during long-term follow-up.

Our present results revealed that imposing a predefined scaffold fiber orientation did not lead to the desired control over the alignment of newly formed collagen in engineered long-term implanted heart valves. This was mainly reflected in the changes in mechanical properties. The higher stiffness in the circumferential alignment in the aTEHV group before implantation was lost as early as after 1 month in vivo, although sample size ($n = 2$) was limited for this follow-up time. Nevertheless, the decrease in stiffness in the circumferential direction in these valves was consistently measured for all valves beyond the 1-month follow-up time as well. The rTEHVs also displayed a certain degree of scaffold anisotropy before implantation, with a preferred fiber direction in the radial direction as a consequence of the electrospinning process for this specific supramolecular elastomer. This mechanical anisotropy in the rTEHVs was also lost after 6 months in vivo, from which point on, all valves displayed isotropic mechanical properties. This was consistent with our previous study, in which any minor anisotropy in implantation mechanical properties was no longer detectable after 6 months (5). After implantation, the mechanical functionality of the valves was determined by the combination of resorbing synthetic scaffold fibers and the newly formed tissue. The observed decrease in stiffness indicated an unexpected loss of integrity of the circumferentially aligned fibers in the aTEHVs, as well as in the other valves beyond 6 months in vivo. This might point to either physical breakage or (accelerated) degradation of the aligned fibers. Although there were no apparent differences between the aTEHV and rTEHV groups in SEM and GPC analysis, it should be noted that these analyses only represented a highly localized section of the leaflet, which might explain why no differences between the groups were detected in the SEM analysis. In addition, GPC data are important to evaluate molecular changes in the material that is leftover, but the data are not indicative of the extent of scaffold resorption (e.g., in terms of mass loss). In previous studies that used in situ TEHVs based on supramolecular elastomers, a highly heterogeneous degradation of scaffolds with the most pronounced degradation in macrophage and/or foreign body giant cell-rich regions was reported (5,6,37). Therefore, although SEM and GPC are valuable to qualitatively assess the mechanisms of resorption, the mechanical tests provide a more representative image of scaffold resorption in the leaflet and its consequence for valve function.

Although it was not possible to elucidate the exact mechanism that caused the overruling of the preimposed scaffold architecture in this study, we speculated that the observed changes in mechanical behavior were most likely a combination of (accelerated) scaffold degradation and the hemodynamic loads, especially considering that all valves in either group attained an isotropic material behavior from 6 months on. It is possible that the altered mechanical loading due to the imposed mechanical anisotropy caused physical breakage of aligned scaffold fibers. However, this was not evident from the in vitro fatigue tests, because the valves typically showed a different failure mode in vitro (macroscopic tearing at the commissure). Moreover, although traditional in vitro functionality tests are important to study initial valve functionality, they cannot account for the in situ remodeling processes that the valves undergo upon implantation, the latter being particularly important for these types of resorbable valves, as opposed to permanent prostheses. We previously excluded that mechanical loading alone had an influence of the degradation of the supramolecular elastomeric scaffolds as used in this study (38). Therefore, it is most likely our observations were a combined result of mechanical loading and potentially accelerated scaffold resorption. The latter was supported by recent in vitro work by Wissing et al. (39), who reported on a micro-architecture–dependent degradation of electrospun scaffolds by human macrophages. In that study, an increase in the macrophage-induced oxidative scaffold degradation was observed in elastomeric scaffolds with a large fiber diameter (approximately 6 μm) and an aligned fiber orientation, similar to the architecture of the aTEHVs used in the present study. Concurrently, the supramolecular polymer used to fabricate the valves in this study was previously demonstrated to be mainly susceptible to oxidative degradation (40). This was confirmed by the qualitative assessment of local scaffold degradation via SEM on our valves, which displayed extensive fiber cleavage from 6 months on. The speculation that local mechanical cues, like stresses and strain, dominated the endogenous remodeling processes over the preimposed scaffold anisotropy was in line with previously reported findings of the vascular scaffolds used

by Zhu et al. (41). They revealed that successful guidance of in situ neotissue organization by circumferentially aligned fibers could only be achieved in compliant arterial grafts with appropriate mechanical loads but not in stiff arterial grafts with aligned fibers, because the former was associated with favorable macrophage polarization and extracellular matrix deposition by contractile vascular smooth muscle cells (41). Similar observations were recently reported by Kryhauw et al. (42), who showed that the predefined circumferential alignment of scaffold fibers in vascular grafts did not lead to the desired control over tissue formation in vivo. A substantial part of the endogenously formed neo-tissue was deposited as a pannus layer on top of the scaffold, rather than in between the scaffold fibers. In these superficial layers, contact guidance by the scaffold was expected to be limited and the alignment of the collagen in those layers was likely to be influenced by the local mechanical loads. These included the wall shear stress on the surface of the leaflet, which was recently shown to affect collagen organization in an in vitro model (22). Numerical modeling of the transient local stresses and strains in aTEHVs and rTEHVs, as well as comprehensive phenotypical analysis of the associated local cellular infiltrates (including immune cells) (43) would be of great added value to further elucidate the combined effects of microstructure and hemodynamic loads on the regenerative processes in the valves.

In general, all valves showed a progressive and ongoing transformation from synthetic scaffold to viable tissue, as exemplified by progressive scaffold degradation and increases in DNA, glycosaminoglycan, and collagen, similar to previous reports (5,6). This was also reflected by the explantation mechanical properties, which generally transitioned from a predominantly linear (scaffold-dominated) to a more nonlinear (more native-like) stress–strain behavior for both scaffold types. More specifically, the elastic moduli at low strains decreased over time, which was indicative of scaffold degradation, whereas the elastic moduli at high strains increased, which was indicative of tissue deposition. It should be noted that there was still abundant scaffold material at 12 months, which was in line with our previous results (5). A longer follow-up time is warranted to investigate how the valve will function and develop when the synthetic scaffold material is completely resorbed. In general, the observed process of endothelialization in this study was similar to our previous study (5), although in the present study, endothelialization tended to be more complete at the ventricular side at 6 months compared with this previous work.

The overall stiffness at 12 months tended to be higher for aTEHVs compared with that of rTEHVs. Because there were no apparent differences in collagen amount and organization, we speculate that this might have been caused by differences in collagen cross-link density between rTEHVs and aTEHVs. This was previously shown to directly correlate to valve biomechanical behavior (44). However, it is not clear as to why the stiffness of the aTEHVs was higher as that of the rTEHVs at 12 months, considering that the stiffnesses were similar at 6 months; similar remodeling after that point should be expected. We speculate that it might have been caused by transient differences in the opening and closing dynamics of the aTEHVs compared to that of the rTEHVs, although this requires further research. This speculation is supported by the finding of extensive degradation of both the polymer and its alignment at 6 months (**Figure 5**) combined with the finding that collagen deposition within the polymer was not observed until 12 months (**Figure 6**). In addition, all valves displayed relatively high pressure gradients caused by a mismatch in the size of the valve and the annulus. Although the valves in both groups showed an increasing trend in pressure gradient over time, which was not statistically significant, the aTEHV group showed an overall trend of higher systolic pressure gradients, which might have been caused by the tendency for increased leaflet stiffness in this group. Considering a stable pulmonary valve annulus and animal weight increase in 12 months in the rTEHV and aTEHV groups, respectively, the increasing trend for the systolic pressure gradients over time, in general, was at least partially explained by somatic growth of the animals. No severe regurgitation was seen on TTE during the study in any of the animals. However, epicardial echo at time of explantation did show 2 valves with severe regurgitation. This discrepancy could be due to the supine position of the sheep and a fully opened thorax in which the epicardial echo was performed. Thoracotomy is known to alter thoracic pressure and cardiac filling (45) and a concomitant decrease in mean arterial pressure (46) and valve function. Therefore, the TTEs during follow-up were considered the most reliable results in the clinically most relevant conditions. The main reason to perform epicardial echo was to evaluate the valve leaflet mobility, which in our hands, was easier in an epicardial window. Based on the TTE, the aTEHVs showed earlier signs of moderate regurgitation.

Interestingly, we detected substantial amounts of (tropo)elastin in the explanted valves, although this

only led to marginal formation of mature elastic fibers. Functional elastic fiber formation is a complex process that entails the incorporation of cross-linked tropoelastin packages into a microfibrillar network (47). Unexpectedly, most valves in this study also displayed various degrees of mineralization, from 6-month follow-up. We thought these were calcium deposits. This was in contrast to our previous work, in which no signs of calcification were observed in any of the valves after 12 months in the sheep model (5). The cause of this discrepancy remains to be elucidated, although it is important to note that the valves in the present study were fabricated from a different kind of polymer, with a higher stiffness. We are currently investigating if the observed mineralization was a purely material-dependent phenomenon or whether it was related to local hemodynamic loads. Moreover, the synthetic valves in our previous study were seeded with fibrin gel before implantation. Previous studies proposed that cross-linked fibrin had anti-thrombogenic properties (48) and that it stimulated the polarization of macrophages toward a pro-regenerative (M2) type (49). Based on these reports, it is plausible that the pre-seeded fibrin played a protective role in preventing valvular calcification in our previous study, although this warrants further research. These discrepancies in outcome, compared with our previous study, emphasize that minor material modifications can have large effects on the in vivo remodeling, including adverse remodeling events (e.g., calcification).

Another important finding of this study was the observed valve-to-valve variability, regardless of the study group. This variability was observed both on the macroscopic and the microscopic levels (Supplemental Figures S3 to S5). Macroscopically, at 1 month, all valves showed pliable and smooth leaflets, whereas from 6 months on, we saw valves with pliable, intact leaflets, as well as valves with small tears and/or irregularities. We saw some minor extent fusion of the belly of the leaflet with its surroundings in some of the valves. From a mechanical point of view, these leaflets were vulnerable to tearing due to inhomogeneous distribution of the loads. Microscopically, variability between valves was evident in terms of the collagen deposition and alignment, as well as in extent of cellularization (Supplemental Figures S3 to S5). Such variability between implantations was also observed in previous studies using resorbable synthetic TEHVs (5,6,37), as well as in vascular grafts (50). For example, a recent study by Fioretta et al. (37) displayed variability between valves of the same type, but also between leaflets within the same valve in minimally invasively delivered supramolecular elastomeric valves. This so far unexplained and unpredictable variability is a critical point of attention with respect to the translation of this technology into a robust and safe clinical treatment. Although it is possible that variations in systemic conditions between animals contribute to causing variability, minor variations in the scaffold fabrication procedure and the implantation might also have large consequences in vivo. This was exemplified by the study by Emmert et al. (16), who showed that misplacement of valves or suboptimal valve geometry could lead to strain distributions over the valve that stimulated adverse remodeling (e.g., leaflet retraction), rather than functional remodeling. Moreover, this study highlighted the power of computational modeling to predict in vivo remodeling. However, it should be noted that that specific computational model did not account for the presence of synthetic scaffold material, and thus, was not directly applicable to predict the in vivo remodeling of synthetic TEHVs. To achieve the latter, inspiration might be drawn from in silico models as recently described by Szafron et al. (51,52) to predict in situ remodeling of resorbable synthetic blood vessels. These models do account for the influence of a synthetic scaffold and the associated inflammatory response on the formation and remodeling of tissue. However, as also highlighted in these studies, mechanistic in vitro data aimed to elucidate the balance among inflammation and scaffold degradation, and tissue formation in well-controlled mechanical conditions (53–55) is required to serve as input for such models to improve their predictive power.

STUDY LIMITATIONS. The present study had several limitations. Due to financial and ethical constraints, the sample size per group was small, making it difficult to draw strong conclusions. Nevertheless, availability of long-term in vivo data on resorbable synthetic heart valves are limited, and, as such, the observations in this study valuably contributed to our overall understanding of in situ heart valve tissue engineering using resorbable synthetic valves. In an effort to maximize the information gained from this study, we opted for a rather broad set of analyses, including mechanical tests, SEM, GPC, en face imaging, histology, and biochemical assays. However, because the available material from a single valve was limited, the inherent consequence was that it was not possible to perform all these analysis on each leaflet of the valve, which could be important to assess

JACC: BASIC TO TRANSLATIONAL SCIENCE VOL. 5, NO. 12, 2020
DECEMBER 2020:1187–206

variability, as previously suggested (37,56). Moreover, because the results were unexpected, the underlying processes largely remain to be elucidated, because they require dedicated analyses for which the study was not designed a priori. One of our avenues of research is aimed at a much more extensive histopathological analysis of the explantation material to map the local inflammatory and regenerative processes using a recently reported dedicated sheep-specific antibody panel (43). Finally, although the microstructural design of the aTEHVs in this study was inspired by the circumferential direction of collagen in the native valve fibrosa, our design was highly simplified because it only captured the fibrosa layer of the valve, but not, for example, the ventricularis, with radially aligned elastin. More sophisticated, layered, bio-mimicking TEHVs are under development by other groups (33,34), and it would be highly interesting to investigate their long-term in vivo behavior.

CONCLUSIONS

The effect of the predefined scaffold architecture did not lead to the desired control over the organization of regenerated tissue, as governed by the in vivo remodeling processes. These unexpected findings highlight the need for a more in-depth understanding of the long-term in situ remodeling processes in large animal models to improve predictability of outcome and allow for rational scaffold design.

ACKNOWLEDGMENTS The authors would like to acknowledge Bente de Kort for performing the elastin assay, Marloes Janssen-van den Broek and Dr. Vivian Mouser for their expert help with the biaxial tensile tests, and Dr. Mark van Turnhout for his expert help in the quantifications of collagen and scaffold alignment.

AUTHOR DISCLOSURES

This research forms part of the iValve-II project, powered by Health ~ Holland, top sector Life Sciences and Health (Grant number TTTI1403B), supported by the Dutch Ministry of Economic Affairs. This work was supported by the Netherlands Cardiovascular Research Initiative (CVON 2012-01): The Dutch Heart Foundation, Dutch Federation of University Medical Centers, the Netherlands Organization for Health Research and Development, the Royal Netherlands Academy of Sciences, and by the Gravitation Program "Materials Driven Regeneration," funded by the Netherlands Organization for Scientific Research (024.003.013). Dr. Aikawa is supported by grants from the National Institutes of Health (R01 HL114805, R01 HL136431, R01 HL147095). Dr. Bouten is a shareholder of Xeltis BV. Drs. Tristan and Mes are employees of Suprapolix BV. Dr. Brugmans is an employee of Xeltis BV. All other authors have reported that they have no relationships relevant to the contents of this paper to disclose.

ADDRESS FOR CORRESPONDENCE: Dr. Carlijn V.C. Bouten, Department of Biomedical Engineering, Eindhoven University of Technology, P.O. Box 513, 5600 MB Eindhoven, the Netherlands. E-mail: c.v.c.bouten@tue.nl. OR Dr. Jolanda Kluin, Department of Cardiothoracic Surgery, Amsterdam University Medical Center, Meibergdreef 9, 1105 AZ Amsterdam, the Netherlands. E-mail: j.kluin@amsterdamumc.nl.

PERSPECTIVES

COMPETENCY IN MEDICAL KNOWLEDGE: In situ tissue engineering has gained more and more attention for heart valve replacement therapy. Implantation of a bare degradable valve scaffold is an affordable and practical application, and therefore, attractive for clinical use. However, to get the valve to the patient, knowledge of the in vivo interactions between the passive (scaffold microarchitecture) and active (hemodynamic loads) cues need to be unraveled. This will enable us to optimize the architecture of the neo-tissue that is formed. This study showed that pre-alignment of the fibers of the scaffold alone using this polymeric material was not able to guide the neo-collagen alignment in a more native-like direction.

TRANSLATIONAL OUTLOOK: In the effort to control the engineering of a living heart valve, we need a thorough understanding of how cells respond and interact with the scaffold material and environmental in vivo circumstances. It remains difficult to identify the relative importance of each (or combinations) of the involved factors. The observed cases of variability between valves, which is concurrent to previous reports, is an important point of attention in terms of safety for clinical translation. This also holds for the observed cases of adverse remodeling (i.e., calcification), although it remains to be elucidated to what extent the observed mineralization will lead to clinically relevant safety issues. In silico experiments, which are driven by in vitro and in vivo obtained data, might be helpful to more reliably predict in vivo outcomes. In addition, the body of long-term in vivo data for resorbable synthetic valves is relatively small to date. Obtaining additional in vivo data with more extensive analysis of the in vivo processes will be indispensable, and longer follow-up times are warranted to establish the functionality and remodeling of the valves when all synthetic scaffold material has been resorbed, albeit its practical, financial and ethical limitations.

REFERENCES

1. Oomen PJA, Loerakker S, van Geemen D, et al. Age-dependent changes of stress and strain in the human heart valve and their relation with collagen remodeling. Acta Biomater 2016;29:161–9.

2. Ayoub S, Ferrari G, Gorman RC, Gorman JH, Schoen FJ, Sacks MS. Heart valve biomechanics and underlying mechanobiology. Compr Physiol 2016;6:1743–80.

3. Chester AH, El-Hamamsy I, Butcher JT, Latif N, Bertazzo S, Yacoub MH. The living aortic valve: from molecules to function. Glob Cardiol Sci Pract 2014;2014:52–77.

4. Hinton RB, Lincoln J, Deutsch GH, et al. Extracellular matrix remodeling and organization in developing and diseased aortic valves. Circ Res 2006;98:1431–8.

5. Kluin J, Talacua H, Smits AIPM, et al. In situ heart valve tissue engineering using a bioresorbable elastomeric implant – from material design to 12 months follow-up in sheep. Biomaterials 2017;125:101–17.

6. Bennink G, Torii S, Brugmans M, et al. A novel restorative pulmonary valved conduit in a chronic sheep model: mid-term hemodynamic function and histologic assessment. J Thorac Cardiovasc Surg 2018;155:2591–601.e3.

7. Bouten CVC, Smits AIPM, Baaijens FPT. Can we grow valves inside the heart? Perspective on material-based in situ heart valve tissue engineering. Front Cardiovasc Med 2018;5:54.

8. Wissing TB, Bonito V, Bouten CVC, Smits AIPM. Biomaterial-driven in situ cardiovascular tissue engineering—a multi-disciplinary perspective. NPJ Regen Med 2017;2:18.

9. Smits AIPM, Bouten CVC. Tissue engineering meets immunoengineering: prospective on personalized in situ tissue engineering strategies. Curr Opin Biomed Eng 2018;6:17–26.

10. da Costa FDA, Etnel JRG, Charitos EI, et al. Decellularized versus standard pulmonary allografts in the Ross procedure: propensity-matched analysis. Ann Thorac Surg 2018;105:1205–13.

11. Iop L, Bonetti A, Naso F, et al. Decellularized allogeneic heart valves demonstrate self-regeneration potential after a long-term preclinical evaluation. PLoS One 2014;9:e99593.

12. Neumann A, Sarikouch S, Breymann T, et al. Early systemic cellular immune response in children and young adults receiving decellularized fresh allografts for pulmonary valve replacement. Tissue Eng Part A 2014;20:1003–11.

13. Driessen-Mol A, Emmert MY, Dijkman PE, et al. Transcatheter implantation of homologous "off-the-shelf" tissue-engineered heart valves with self-repair capacity: long-term functionality and rapid in vivo remodeling in sheep. J Am Coll Cardiol 2014;63:1320–9.

14. Motta SE, Lintas V, Fioretta ES, et al. Human cell-derived tissue-engineered heart valve with integrated Valsalva sinuses: towards native-like transcatheter pulmonary valve replacements. NPJ Regen Med 2019;4:14.

15. Weber B, Dijkman PE, Scherman J, et al. Off-the-shelf human decellularized tissue-engineered heart valves in a non-human primate model. Biomaterials 2013;34:7269–80.

16. Emmert MY, Schmitt BA, Loerakker S, et al. Computational modeling guides tissue-engineered heart valve design for long-term in vivo performance in a translational sheep model. Sci Transl Med 2018;10.

17. Syedain Z, Reimer J, Schmidt J, et al. 6-Month aortic valve implantation of an off-the-shelf tissue-engineered valve in sheep. Biomaterials 2015;73:175–84.

18. Reimer J, Syedain Z, Haynie B, Lahti M, Berry J, Tranquillo R. Implantation of a tissue-engineered tubular heart valve in growing lambs. Ann Biomed Eng 2017;45:439–51.

19. Mela P, Hinderer S, Kandail HS, Bouten CVC, Smits AIPM. Tissue-engineered heart valves. In: Kheradvar A, editor. Principles of Heart Valve Engineering. St. Louis, MO: Elsevier, 2019:123–76.

20. Foolen J, Deshpande VS, Kanters FMW, Baaijens FPT. The influence of matrix integrity on stress-fiber remodeling in 3D. Biomaterials 2012;33:7508–18.

21. de Jonge N, Foolen J, Brugmans MCP, et al. Degree of scaffold degradation influences collagen (re)orientation in engineered tissues. Tissue Eng Part A 2013;20:1747–57.

22. Van Haaften EE, Wissing TB, Rutten MCM, et al. Decoupling the effect of shear stress and stretch on tissue growth and remodeling in a vascular graft. Tissue Eng Part C Methods 2018;24:418–29.

23. Aper SJA, van Spreeuwel ACC, van Turnhout MC, et al. Colorful protein-based fluorescent probes for collagen imaging. PLoS One 2014;9:e114983.

24. Li RL, Russ J, Paschalides C, et al. Mechanical considerations for polymeric heart valve development: biomechanics, materials, design and manufacturing. Biomaterials 2019;225:119493.

25. Sohier J, Carubelli I, Sarathchandra P, Latif N, Chester AH, Yacoub MH. The potential of anisotropic matrices as substrate for heart valve engineering. Biomaterials 2014;35:1833–44.

26. Masoumi N, Larson BL, Annabi N, et al. PCL microfibers align human valvular interstitial cells and provide tunable scaffold anisotropy. Adv Healthc Mater 2014;3:929–39.

27. Gaharwar AK, Nikkhah M, Sant S, Khademhosseini A. Anisotropic poly (glycerol sebacate)-poly (ε-caprolactone) electrospun fibers promote endothelial cell guidance. Biofabrication 2014;7:015001.

28. Hosseini V, Evrova O, Hoerstrup SP, Vogel V. A simple modification method to obtain anisotropic and porous 3D microfibrillar scaffolds for surgical and biomedical applications. Small 2018;14:1702650.

29. Capulli AK, Emmert MY, Pasqualini FS, et al. JetValve: Rapid manufacturing of biohybrid scaffolds for biomimetic heart valve replacement. Biomaterials 2017;133:229–41.

30. Tseng H, Puperi DS, Kim EJ, et al. Anisotropic poly(ethylene glycol)/polycaprolactone hydrogel-fiber composites for heart valve tissue engineering. Tissue Eng Part A 2014;20:2634–45.

31. Moreira R, Neusser C, Kruse M, et al. Tissue-engineered fibrin-based heart valve with bio-inspired textile reinforcement. Adv Healthc Mater 2016;5:2113–21.

32. Li Q, Bai Y, Jin T, Wang S, et al. Bioinspired engineering of poly(ethylene glycol) hydrogels and natural protein fibers for layered heart valve constructs. ACS Appl Mater Interfaces 2017;9:16524–35.

33. Saidy NT, Wolf F, Bas O, et al. Biologically inspired scaffolds for heart valve tissue engineering via melt electrowriting. Small 2019;15:1900873.

34. D'Amore A, Luketich SK, Raffa GM, et al. Heart valve scaffold fabrication: Bioinspired control of macro-scale morphology, mechanics and microstructure. Biomaterials 2018;150:25–37.

35. Loerakker S, Argento G, Oomens CWJ, Baaijens FPT. Effects of valve geometry and tissue anisotropy on the radial stretch and coaptation area of tissue-engineered heart valves. J Biomech 2013;46:1792–800.

36. Serrani M, Brubert J, Stasiak J, et al. A computational tool for the microstructure optimization of a polymeric heart valve prosthesis. J Biomech Eng 2016;138:061001.

37. Fioretta ES, Lintas V, Mallone A, et al. Differential leaflet remodeling of bone marrow cell pre-seeded versus nonseeded bioresorbable transcatheter pulmonary valve replacements. J Am Coll Cardiol Basic Trans Science 2020;5:15–31.

38. Van Haaften EE, Duijvelshoff R, Ippel BD, et al. The degradation and performance of electrospun supramolecular vascular scaffolds examined upon in vitro enzymatic exposure. Acta Biomater 2019;92:48–59.

39. Wissing TB, Bonito V, van Haaften EE, et al. Macrophage-driven biomaterial degradation depends on scaffold microarchitecture. Front Bioeng Biotechnol 2019;7:87.

40. Brugmans MCP, Söntjens SHM, Cox MaJ, et al. Hydrolytic and oxidative degradation of electrospun supramolecular biomaterials: in vitro degradation pathways. Acta Biomater 2015;27:21–31.

41. Zhu M, Wu Y, Li W, et al. Biodegradable and elastomeric vascular grafts enable vascular remodeling. Biomaterials 2018;183:306–18.

42. Krynauw H, Buescher J, Koehne J, et al. Tissue ingrowth markedly reduces mechanical anisotropy and stiffness in fibre direction of highly aligned electrospun polyurethane scaffolds. Cardiovasc Eng Technol 2020;11:456–68.

43. Dekker S, van Geemen D, van den Bogaerdt AJ, Driessen-Mol A, Aikawa E, Smits AIPM. Sheep-specific immunohistochemical panel for the evaluation of regenerative and

inflammatory processes in tissue-engineered heart valves. Front Cardiovasc Med 2018;5:105.

44. Balguid A, Rubbens MP, Mol A, et al. The role of collagen cross-links in biomechanical behavior of human aortic heart valve leaflets–relevance for tissue engineering. Tissue Eng 2007;13:1501–11.

45. Komarek J, Mansfeld C. [Effect of thoracotomy on the contractility parameters of the left heart ventrilce in dogs]. Z Kardiol 1975;64:976–83.

46. van Hout GPJ, Teuben MPJ, Heeres M, et al. Invasive surgery reduces infarct size and preserves cardiac function in a porcine model of myocardial infarction. J Cell Mol Med 2015;19:2655–63.

47. Wagenseil JE, Mecham RP. New insights into elastic fiber assembly. Birth Defects Res C Embryo Today 2007;81:229–40.

48. Skarja GA, Brash JL, Bishop P, Woodhouse KA. Protein and platelet interactions with thermally denatured fibrinogen and cross-linked fibrin coated surfaces. Biomaterials 1998;19:2129–38.

49. Hsieh JY, Smith TD, Meli VS, et al. Differential regulation of macrophage inflammatory activation by fibrin and fibrinogen. Acta Biomater 2016:1–11.

50. Khosravi R, Miller KS, Best CA, et al. Biomechanical diversity despite mechanobiological stability in tissue engineered vascular grafts two years post-implantation. Tissue Eng Part A 2015;21:1529–38.

51. Szafron JM, Khosravi R, Reinhardt J, et al. Immuno-driven and mechano-mediated neotissue formation in tissue engineered vascular grafts. Ann Biomed Eng 2018;46:1938–50.

52. Szafron JM, Ramachandra AB, Breuer CK, Marsden AL, Humphrey JD. Optimization of tissue-engineered vascular graft design using computational modeling. Tissue Eng Part C Methods 2019;25:561–70.

53. Van Haaften EE, Wissing TB, Kurniawan NA, Smits AIPM, Bouten CVC. Human in vitro model mimicking material-driven vascular regeneration reveals how cyclic stretch and shear stress differentially modulate inflammation and matrix deposition. Adv Biosyst 2020;4:1900249.

54. Wissing TB, van Haaften EE, Koch SE, et al. Hemodynamic loads distinctively impact the secretory profile of biomaterial-activated macrophages – implications for in situ vascular tissue engineering. Biomater Sci 2020;8:132–47.

55. Battiston KG, Labow RS, Simmons CA, Santerre JP. Immunomodulatory polymeric scaffold enhances extracellular matrix production in cell co-cultures under dynamic mechanical stimulation. Acta Biomater 2015;24:74–86.

56. Mela P. Subject- and leaflet-specific remodeling of polymeric heart valves for in situ tissue engineering. J Am Coll Cardiol Basic Trans Science 2020;5:32–4.

KEY WORDS **cell biology/structural biology, valvular heart disease**

APPENDIX **For an expanded Methods section as well supplemental tables, figures, and videos, please see the online version of this paper.**